Applied Sciences, Computing and Energy, 2(1), 55-69

Integrating Satellite Imagery and Aero-radiometric Datasets in Lithological Discrimination and Detection of Hydrothermal Zones at Ikara and its Environs, North-Central of the Basement Complex, Nigeria

Nana Fatima Abdulmalik*, Bello, Ayoola Yusuf, Mu'awiya Baba Aminu and Christopher Simon Dalom.

Received; 12 November 2024/Accepted : 29 February 2025/Published: 11 March 2025

Abstract: *Aero-radiometric data and Landsat-8 Operational Land Imager data were used to identify different rock types in the research area. Bands 4,3,2 and 6,5,4 of Landsat-8 OLI were used for natural and false colour composites to discriminate lithological units. Bands 7,5,3 was utilized for principal component analysis for further lithological discrimination. In addition to clearly visualize the lithological boundaries and regions of mineralization potentials, the use of aero-radiometric data was equally employed. The aero-radiometric data revealed regions where K, eTh and eU natural radionuclide elements (NORMS) were, generated individually for each NORM. Then, a ternary map was generated which revealed the regions of lithological units of the study area. This correlated with results attained from the Landsat-8 OLI. This revealed that lithologies at the northern parts had K>eU/eTh (migmatites, medium to coarse grained granites and porphyritic granites) and lithologies in the southern parts had eTh/eU>K (porphyroblastic gneiss and augen gneiss). From both Landsat and aero-radiometric maps, the presence of a regional fracture was identified trending NW-SE across the study area. The ternary image and K/eTh ratio revealed zones of possible hydrothermal alterations which was observed along the regional fault and shear zones identified within the study area. This suggested that the zones of hydrothermal alterations were structurally controlled. These were further confirmed on ground study and discovered areas where amethyst mineralization and alluvial cassiterite deposits were once mined.*

Key words: *Landsat-8 OLI Data, Aero-radiometric Data, Lithological Units, Hydrothermal Zones, Fault/Shear Zones.*

Nana Fatima Abdulmalik
Centre for Energy Research and Training, Ahmadu Bello University, Zaria
E-mail: **nanafatima88@gmail.com**
Orcid id: https://orcid.org/0000-0002-7501-8155

Bello, Ayoola Yusuf
Department of Physics, Airforce Institute of Technology, Kaduna
Email: **belloya@afit.edu.ng**

Mu'awiya Baba Aminu
[1]Universiti Sains Malaysia, School of Materials and Mineral Resources Engineering, Nibong Tebal, Penang, Malaysia
[2]Department of Geology, Federal University Lokoja, Lokoja, Kogi State, Nigeria
E-mail:
babaaminum@student.usm.myMuawiya.
babaaminu@fulokoja.edu.ng,
Orcid id: https://orcid.org/0000-0001-5278-153X

Christopher Simon Dalom
Department of GeologyFederal University Lokoja, , Lokoja, Kogi State, Nigeria
E-mail: **simon.christopher@fulokoja.edu.ng**
Orcid id: https://orcid.org/0000-0003-0989-7662

1.0 Introduction

The use of remote sensing, a contemporary technique, gives geoscientists the ability to gather data sets in the form of pictures at various bands. Over the years, it has demonstrated exceptional reliability and outstanding capacity for large-scale geological mapping of a variety of characteristics, as noted by Semere and Ghebreab (2006) and Maged et al. (2009). The Landsat 8 satellite, launched on February 11, 2013, is equipped with two key sensors: the Thermal Infrared Sensor (TIRS) and the Operational Land Imager (OLI). These instruments operate across eleven distinct bands of the electromagnetic spectrum, including the deep blue coastal/aerosol band and the shortwave cirrus band. They cover a range of spectral regions, such as thermal infrared (TIR), shortwave infrared (SWIR), and visible to near-infrared (VNIR) wavelengths. The OLI, as a multispectral sensor, specifically captures data within the SWIR and VNIR spectral ranges.

The level-1T (Terrain Corrected) dataset captured by the Operational Land Imager (OLI) was obtained from NASA's Land Processes Distributed Active Archive Center (LP DAAC). This dataset consists of nine distinct spectral bands, which include three shortwave infrared (SWIR) bands ranging between 1.57 and 2.29 µm, with the Cirrus band being one of them, as well as five visible and near-infrared (VNIR) bands spanning 0.43 to 0.88 µm, including the coastal aerosol band (refer to Tables 1 and 2 for details). Imagery from Landsat 8 OLI is radiometrically calibrated for accuracy, orthorectified for improved spatial alignment, geometrically co-registered, and characterized by a narrower and more refined spectral range to enhance data quality. The readily accessible Landsat 8 OLI scenes, which span 185 x 180 kilometers, are notably high in radiometric resolution of 16 bits. For lithological and mineralogical mapping, hyperspectral data collected from satellites and airborne sensors, such as EO-1 Hyperion and AVIRIS, are widely utilized due to their high spectral resolution, which is particularly advantageous for identifying hydrothermal alteration zones. Additionally, a variety of multispectral sensors, including Terra ASTER, Landsat 5 TM, Landsat 7 ETM+, and Sentinel 2A, are frequently employed for efficient mapping of lithological units (Kruse et al., 2003; Pour and Hashim, 2012; Pournamdari et al., 2014; Jellouli et al., 2019; Adiri et al., 2019). The Landsat 8 Operational Land Imager (OLI) and Thermal Infrared Sensor (TIRS) operate within wavelengths ranging from 0.43 to 1.38 micrometers, capturing images across nine spectral bands. Among these, Bands 1 through 7 and Band 9 offer a spatial resolution of 30 meters, while Band 8 (panchromatic) provides a sharper resolution of 15 meters. The newly introduced Band 1 (ultra-blue) is especially suited for coastal and aerosol-related studies, whereas Band 9 is tailored for cirrus cloud detection.

There are numerous scientific domains where radiometric maps and surveys can be used. For structural geology, geochemical mapping, and mineral prospecting, they preserve their geological and geophysical data, which also makes it possible to compare geological features across wide geographic areas (Aminu et al., 2022a; Agboola et al., 2024; Chijioke-Churuba, 2023; Chijioke-Churuba, 2024; Amarachukwu et al., 2024). In order to find radioelements like uranium, thorium, and potassium in different lithologies, aeroradiometric data is gathered using airborne gamma-ray spectrometers, which are geophysical instruments installed on aircraft that fly close to the surface of the Earth. Even though the gamma-ray method was originally developed for geoscientific purposes, The decay series of potassium, uranium, and thorium are the primary sources of gamma rays with sufficient energy and intensity to be detectable through gamma-ray spectrometry. This capability stems from their significant natural abundance in the environment.

According to Minty (1997) and the IAEA (2003), the average concentrations of these elements in the Earth's crust are approximately 2–2.5% for potassium, 2–3 ppm for uranium, and 8–12 ppm for thorium.

The simultaneous presence of different K and eTh concentrations in mineralized zones may be a sign of Th migration in a system that has undergone hydrothermal alteration (Silva et al., 2003). Hydrothermal changes are linked to both low thorium and high potassium contents, especially in a number of ore deposits (Ostrovskiy, 1975). To be able to find hydrothermal alteration zones, K/eTh ratio maps are created. Finding regions with possible mineralization is made easier by the way mineralization processes alter the radioelement concentrations of the crust (Dickson and Scott, 1997). Kettles et al. (2000) highlight that the ratio patterns of potassium (K), equivalent uranium (eU), and equivalent thorium (eTh) in surface rocks can magnify subtle changes in elemental concentrations. These variations are often linked to lithological differences or alteration processes associated with mineralization. Tri-lateral plots, also called Ternary images, are color composite maps composed of various radio-elements that usually give a better impression of a region's geology and correspond to the region's actual lithological discrimination or spread (IAEA, 2003; Salem et al., 2005). Using Landsat-8 OLI and aeroradiometric data, the underlying lithologies and hydrothermal alteration zones in the chosen area were created, examined, and interpreted.

1.1 *Location and geologic setting of study area*

The research location for this study is the North-Central Nigerian Basement Complex, which includes parts of Kano and Kaduna states. The region is situated between longitudes 08° 00' 00" E and 08° 30' 00" E, and latitudes 11° 00' 00" N and 11° 30' 00" N (Fig. 1). It is scaled at 1 in 100,000 and has an area of about 3,031 square kilometers. The Migmatite-Gneiss Complex and older granites provide the majority of its support.

The Nigerian Basement Complex formed through the collision of the Congo Craton, the West African Craton, and the East Saharan Block (Black et al., 1979; LeBlanc, 1981; Nanfa et al., 2022; Aminu 2022b). McCurry (1976) proposed that it represents the southern extension of the Central Hoggar and is commonly referred to as the Neoproterozoic Trans-Saharan Belt. Between 750 and 500 million years ago, repeated collisions of island arcs, sedimentary basins, and continental fragments contributed to the formation of this belt, which extends from North Africa to Brazil (Wright et al., 1985; Boullier, 1991; Caby, 1989; Ajibade & Wright, 1989). These collisions induced significant deformation, metamorphism, and structural alterations. During the Pan-African Orogeny (approximately 600 ± 150 million years ago), the region containing the Nigerian Basement Complex was reactivated by the extrusion of alkaline to calc-alkaline volcanic materials (Holt et al., 1978; McCurry & Wright, 1977). The belt is situated northwest of the Congo Craton, east of the West African Craton, and south of the Tuareg Shield, as described by Burke and Dewey (1972), Turner (1983), and Fitches et al. (1985). The region is composed of older crustal materials dating back to the Archean and Palaeoproterozoic eras (Oversby, 1975; Grant, 1970; Grant et al., 1972).

The Nigerian Basement Complex encompasses a large portion of the country's eastern, southern, northwestern, southwestern, and north-central regions. Its primary lithostratigraphic units are Schist Belts, Migmatite-Gneisses, and the Older and Younger Granite Complexes (Woakes et al., 1987) (Fig. 2). This complex is separated into Jurassic Younger Granites, Tertiary to Recent Sediments, Tertiary Volcanics, Precambrian Basement Rocks, and Cretaceous Sediments (Obaje 2009). Interestingly, sediments from the Cretaceous to Recent periods make up around half of the Basement Complex (Woakes et al., 1987). Conjugate fault networks that connect and counteract previous mylonitic shear zones are among the structural characteristics of the Basement Complex in northwest Nigeria (Ball, 1980).

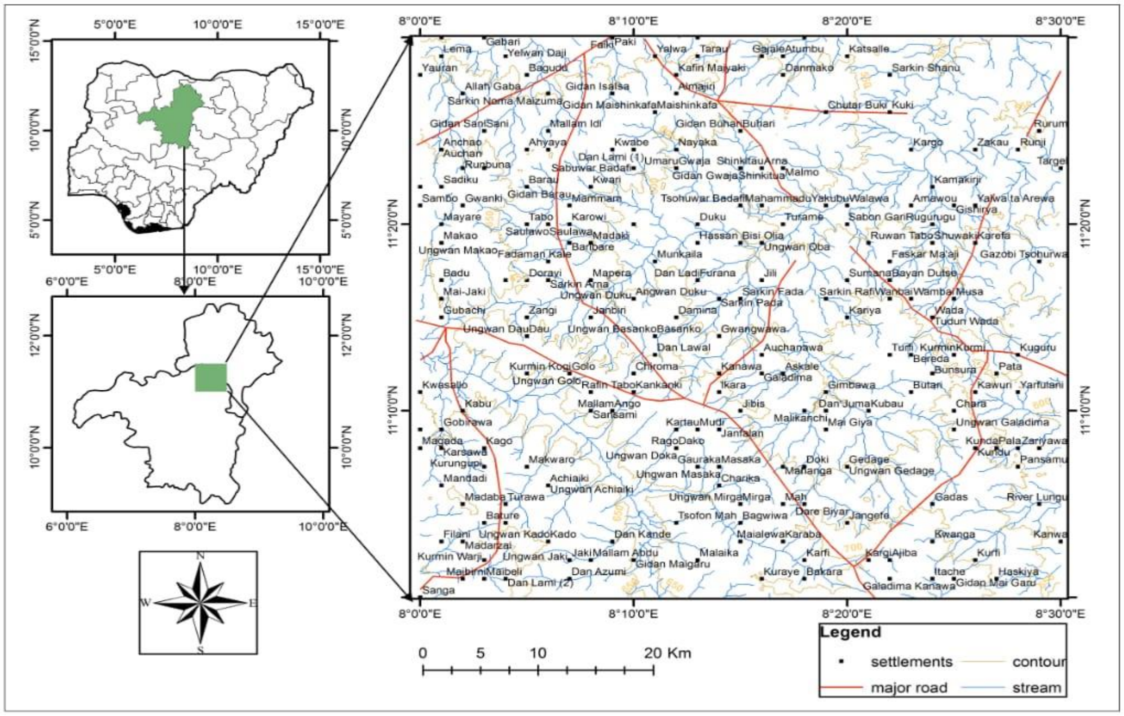

Fig. 1: A map of Nigeria that displays the states and research areas.

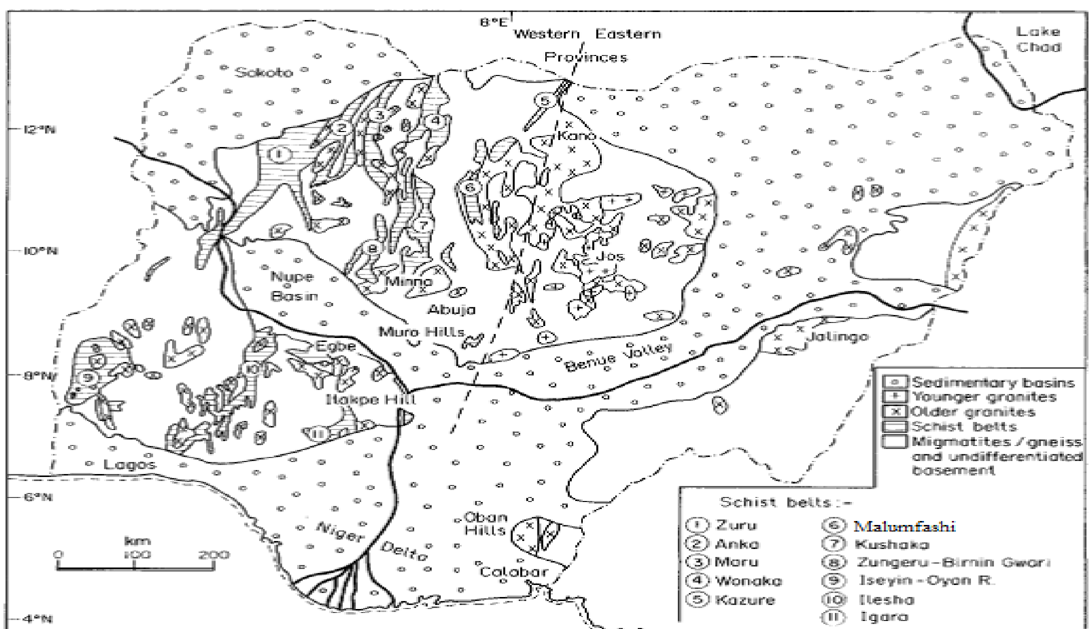

Fig. 2: A geological map of Nigeria that displays the sedimentary basins and the Precambrian Basement Complex (Woakes et al., 1987)

2.0 Materials and Methods

The Landsat-8 Operational Land Imager (OLI) satellite image bands 2, 3, 5, 6, and 7 were obtained from the Earth Explorer database (https://earthexplorer.usgs.gov/). These specific bands correspond to various regions of the electromagnetic spectrum, such as visible light (bands 2, 3, and 4), near-infrared (band 5), and shortwave infrared I and II (bands 6 and 7). Geological features and existing rock types were identified using principal component analysis and various band combinations (natural and artificial color). Between two Landsat pictures, namely C2:T1, from the Collection and Real-Time (Tier) collections, is the study region. Processing was done at the L2SP collection level using the Landsat-8 OLI sensor, which was utilized to gather data on February 2, 2021. 188-052 and 189-052 are the rows and pathways that relate to the study region.

A composite map was created after scenes were pre-processed by mosaicking them using ArcGIS software, followed by the extraction of the research area's coordinates. The bands to be employed have previously been specified, and the following table lists their spectral and spatial resolution properties. Due to the fact that the study region is located between two Landsat series scenes, Collection and Real Time (Tier), at 2 and 1 (C2:T1), respectively, the Landsat-8 OLI sensor was utilized for the acquisition. The sensor was obtained on February 2, 2021, with a processing collection level of L2SP. The study was drawn from the 188-052 and 189-052 rows and pathways. Before the coordinates of the research region were taken out to create a composite map, the scenes were pre-processed by mosaicking them using ArcGIS software.

The bands selected for the analysis, along with their spectral and spatial resolution characteristics, are allocated to different color channels for every color combination process, as previously explained: the first band is positioned on the "R" (Red), the subsequent one on the "G" (Green), and the final band on the "B" (Blue). After loading and saving the photographs, the program exports them using Global Mapper software to determine the precise coordinates of the research area because the images are georeferenced. In order to calculate new statistics, principle Component Analysis (PCA) rotated the forward principle component after first choosing the principal component, just like in the false-color composite. Prior to loading RGB, the bands' spatial subsets were selected in order to execute the band combinations. This was done to further increase the areas that contain particular types of rock and to support the location of important faults and fractures in the area.

Using the same fictitious picture composite format, spatial subsets for the bands were chosen for the principle component analysis prior to loading RGB. The principal component was then rotated forward to calculate fresh statistics. The bands 3, 5, and 7 were selected because they produced less noise. This was used to further differentiate between different rock units within the research area.

For the Ikara Sheet 103, the Nigeria Geological Survey Agency provided aeroradiometric data at a scale of 1:1,000,000. With the airplane flying in a 135°/315° direction, the data gathering process included line spacing, tie-line, and flying height of 500, 5000, and 80 meters, respectively. The software program Oasis Montaj was used to import the gridded data for processing. While a ternary map was made to give a more accurate geological depiction of the region and help categorize different rock units, a K/eTh map was made to show possible areas of hydrothermal alterations (Salem et al., 2005; Youssef and Elkhodary, 2013; Wemegah et al., 2015; Ahmed, 2018; Elkhateeb and Abdellatif, 2018; Ogungbemi et al., 2018; Lawal, 2020). The concentrations of uranium (eU), thorium (eTh), and potassium (K) radionuclides across the lithological units of the study area are clearly represented in these maps.

Histogram equalization was used to improve the radioelements' regional distribution in the survey area and facilitate the identification or differentiation of lithological assemblages. To make sure the radioelement abundance could be seen clearly, the saturation (the color's intensity) and hue (the color's primary wavelength) were changed. Nevertheless, the CMY color model was not used because of its drawbacks, which included limiting the eU contrast enhancement and prohibiting the best possible data stretching without changing the radioelement ratios (IAEA, 2003).

Additionally, radiometric data that correlates with rock units and their structural patterns can be used to identify between different lithologies. Certain radioelements are more abundant in certain rocks whereas others are less abundant. The concentration of uranium is higher in older granites than in potassium and thorium, the concentration of potassium is higher in metasedimentary rocks than in uranium and thorium, and the concentration of thorium is higher in metavolcanics and metagabbros than in uranium and potassium (Youssef and Elkhodary, 2013; Wemegah et al., 2015; Elkhateeb and Abdellatif, 2018).

2.0 Results and Methods

High potassium (K) and low thorium (eTh) concentrations are often related with changes in various ore deposits (Ostrovskiy, 1975). The mobilization of thorium in hydrothermally changed systems, however, is indicated by the rise in eTh intensity and K% observed in some mineral deposits (Silva et al., 2003). This result implies the importance of the K/eTh ratio map for determining potential hydrothermal alteration zones. A map for identifying lithological section and hydrothermal alterations to the area was created by analyzing the radioelements of K, uranium (U), and thorium (Th), also the total count (TC), the K/Th ratio, and a ternary picture.

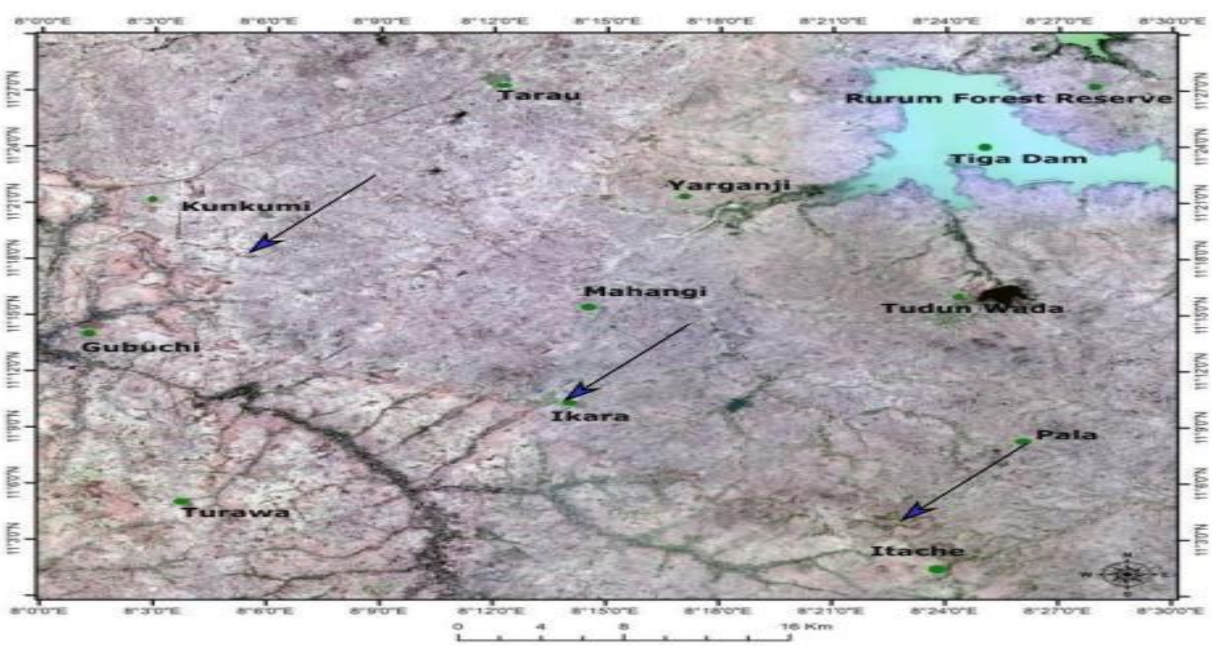

Fig. 3: The natural color composite of bands 4, 3, and 2 is seen in the research area's Landsat image.

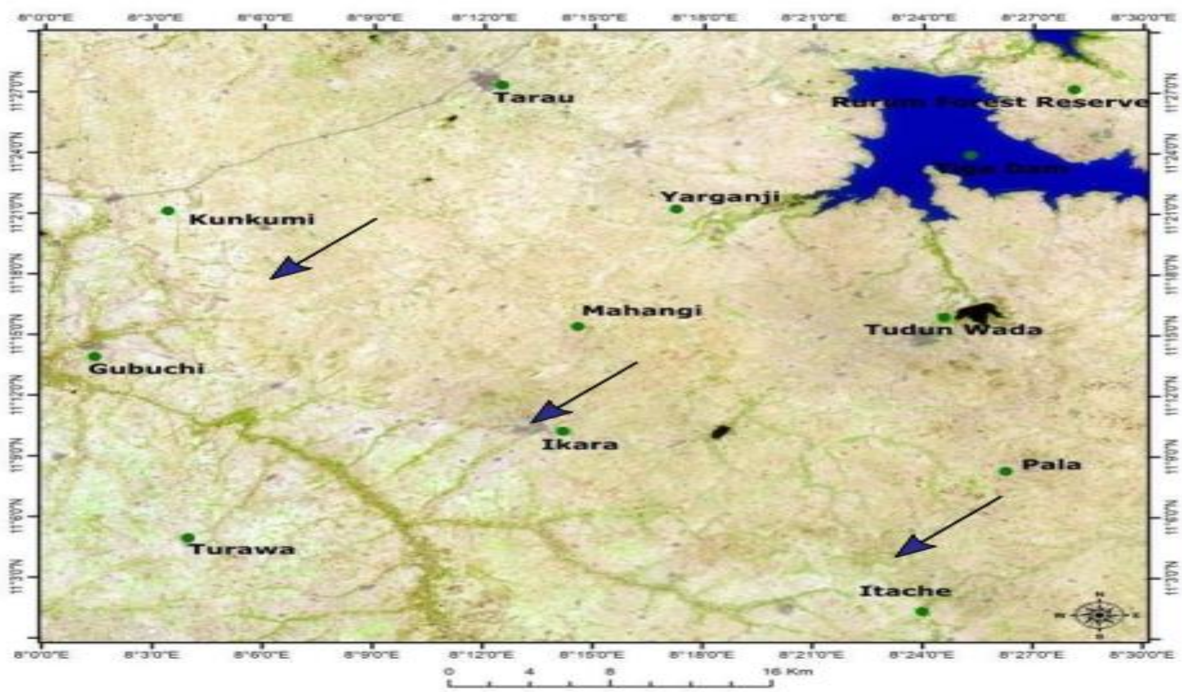

Fig. 4: The combination of bands 6, 5, and 4 (FCC) is shown in the research area's Landsat image..

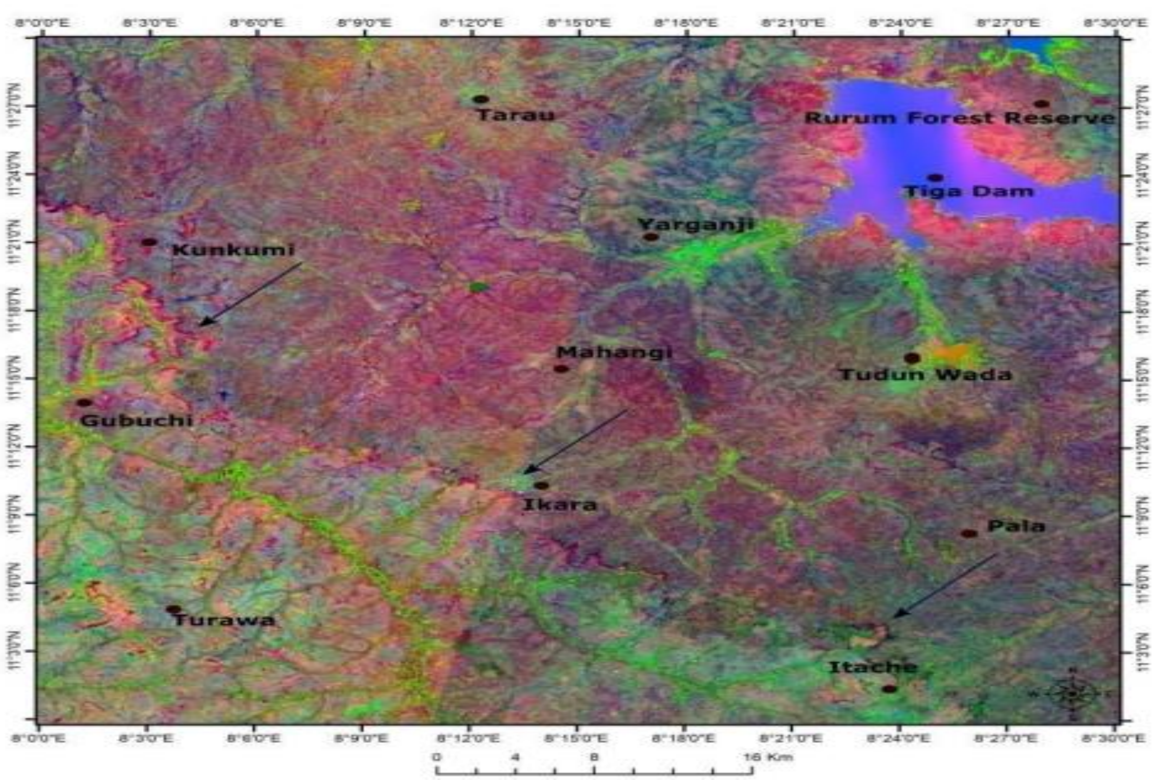

Fig. 5: Analysis of the research area's principal components (bands 7, 5, 3).

From the aeroradiometric data acquired, potassium, thorium and uranium were individually identified across the study area following step by step operations using the software.Gridding was used to interpolate the data into a designated coordinate system because these data are in the form of grids. Therefore, this type of gridding was created in the software using smallest curvature. Each of the elements were selected and displayed, revealing areas with minimum and maximum occurrences of the radionuclides.

In Fig. 6, Potassium was revealed with maximum values at 4.4 and minimum value as low as 0.3, both in percentages (%). The regions with higher potassium occurrence extend northeastward within the research area and trend NW-SE. Coarse porphyritic biotite-hornblende granites and migmatites cover these regions. However, the potassium concentration is low in the southwest, where medium- to coarse-grained biotite granites are found.

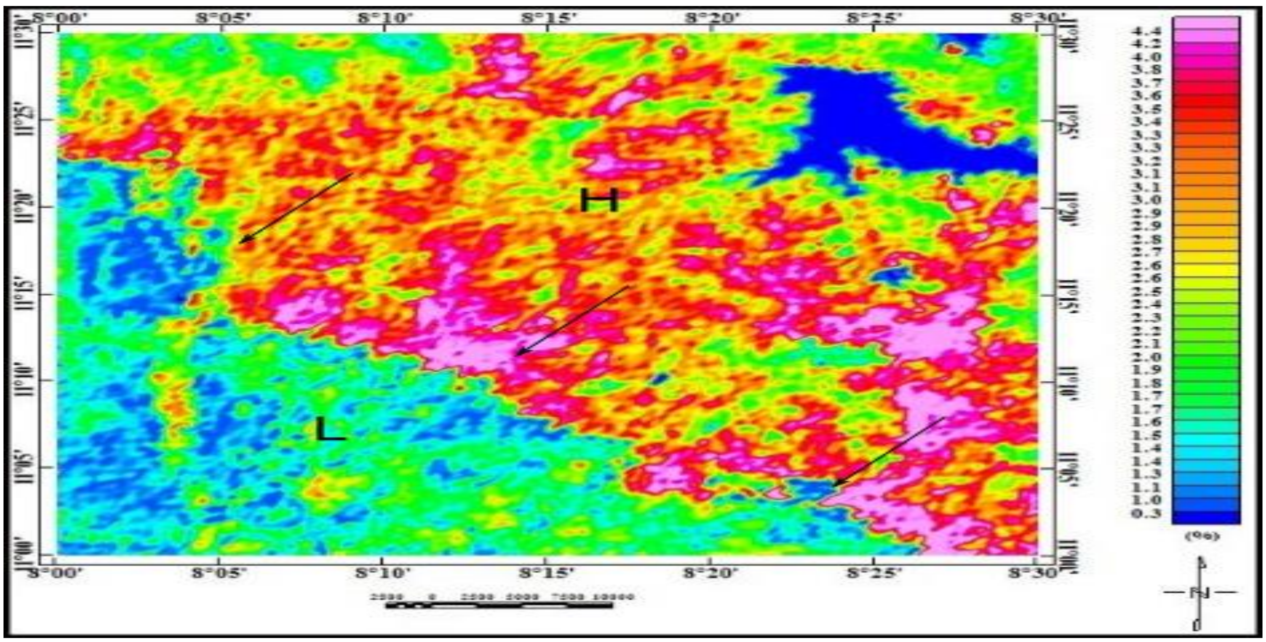

Fig. 6: Aeroradiometric map of study area showing Potassium (K) concentrations in (%).

Thorium on the other hand in Fig. 7 shows to be more, spanning from the central regions towards the southwest. The study area displays less thorium occurrence from northwest, northeast and some portions in the southeast. The maximum value of thorium occurrence is 29.9 and the minimum reveals to be 2.6, both in parts per million (ppm). Medium grained biotite granites and coarse porphyritic biotite-hornblende granites have more of thorium, while areas occupied by migmatites have less occurrence of thorium.

Uranium (eU) occurrence within the study area was displayed and shows high prospects towards the southwest as well, just as observed in the Thorium map (Fig. 8). It occurs dominantly in the southwest, northwest and the east, trending mainly towards the NW-SE. it also occurs in low concentrations at the southeast and northeast. Uranium (eU) is housed within the medium to course grained biotite granites and the biotite hornblende granites with occurrences within the migmatites. The maximum value of uranium within the study area in parts per million (ppm) is 6.9, and the lowest is 1.1. It is also noteworthy to understand that from the maps/images of the radioelements produced below, they were all structurally controlled by NW-SE trending fractures within their zones of occurrence. They are not in mineable quantities.

The K/eTh ratio map in Fig. 9 displays the locations of hydrothermal alteration zones. These zones were primarily found along the research area's regional fracture cross-cut. This fracture is also responsible for the clear demarcation between eU/eTh and K>eU/eTh zones of concentration. The zones with strong/high to highest indication of hydrothermal alteration lies along the regional NW-SE trending fracture, shaded in red/pink with a %/ppm of (0.194-0.329); the zones with moderate indication in orange/yellow shade has a %/ppm of (0.188-0.143); while the zones with the low to lowest indication of hydrothermal activities in green/blue shade has a %/ppm of (0.041-0.138). the zones with strong K/eTh indicator signifies potassium to be higher than thorium. While the zones with low K/eTh indicates potassium to be of low concentration and thorium of high concentration.

Tri-lateral image was produced from aeroradiometric data whereby signals were derived from particularly lithologies and structural features from the subsurface of 80 metres. The image was enhanced and displayed in three colour composition (R: G: B: = K: Th: U) as potassium (K), thorium (Th) and uranium (U) are the 3 main radioactive elements detected and displayed in the image. The 3 elements (K, U and Th) are also referred to as radionuclide of which their concentrations (radionuclide concentrations) varied from place to place. K>U/Th at the northern parts underlain by migmatites, gneisses, medium to course grained, medium to course grained biotite granites and porphyritic granites. U/Th>K at the southern parts underlain by some migmatitic-gneisses, porphyroblastic gneisses, porphyritic fine-grained granites and medium to course grained granites (Fig. 10).

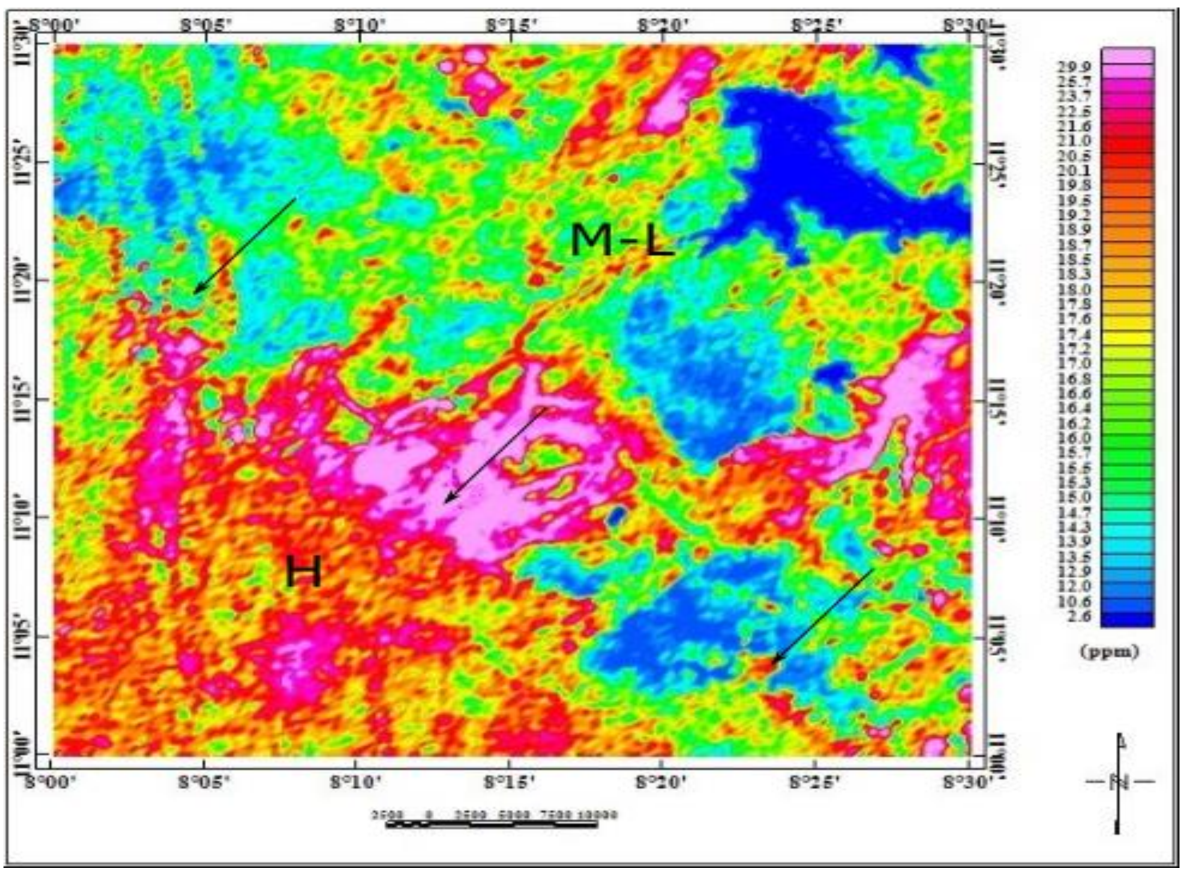

Fig. 7: Aeroradiometric map of study area displaying (eTh) concentration in ppm.

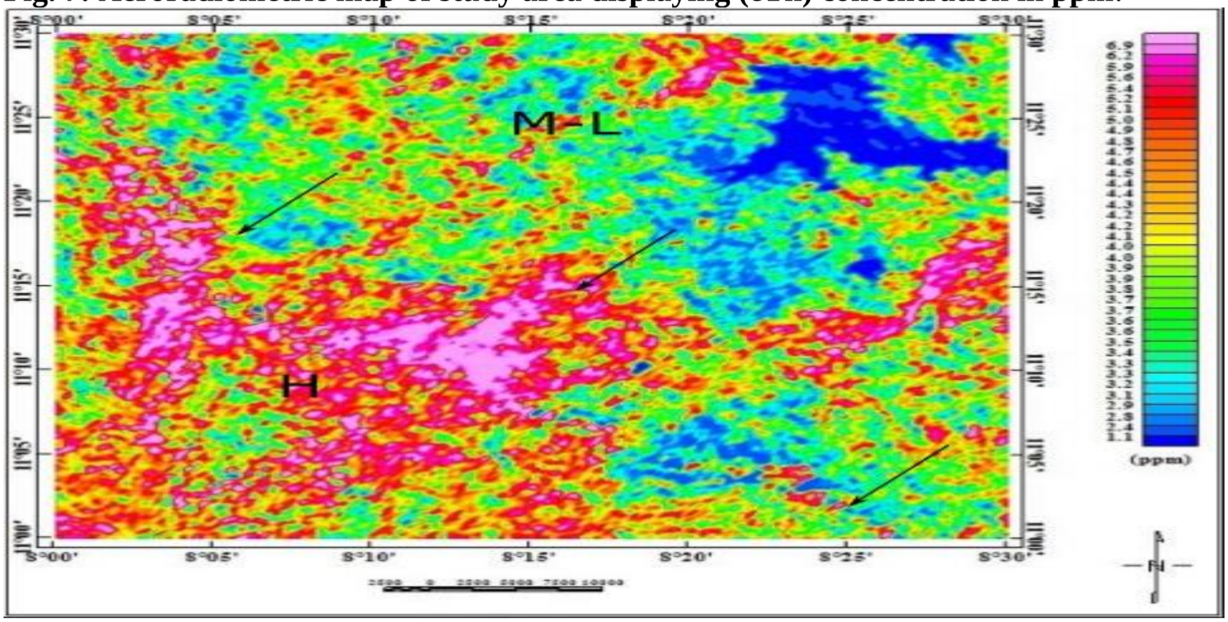

Fig. 8: Aeroradiometric map of study area showing Uranium (eU) concentration in ppm.

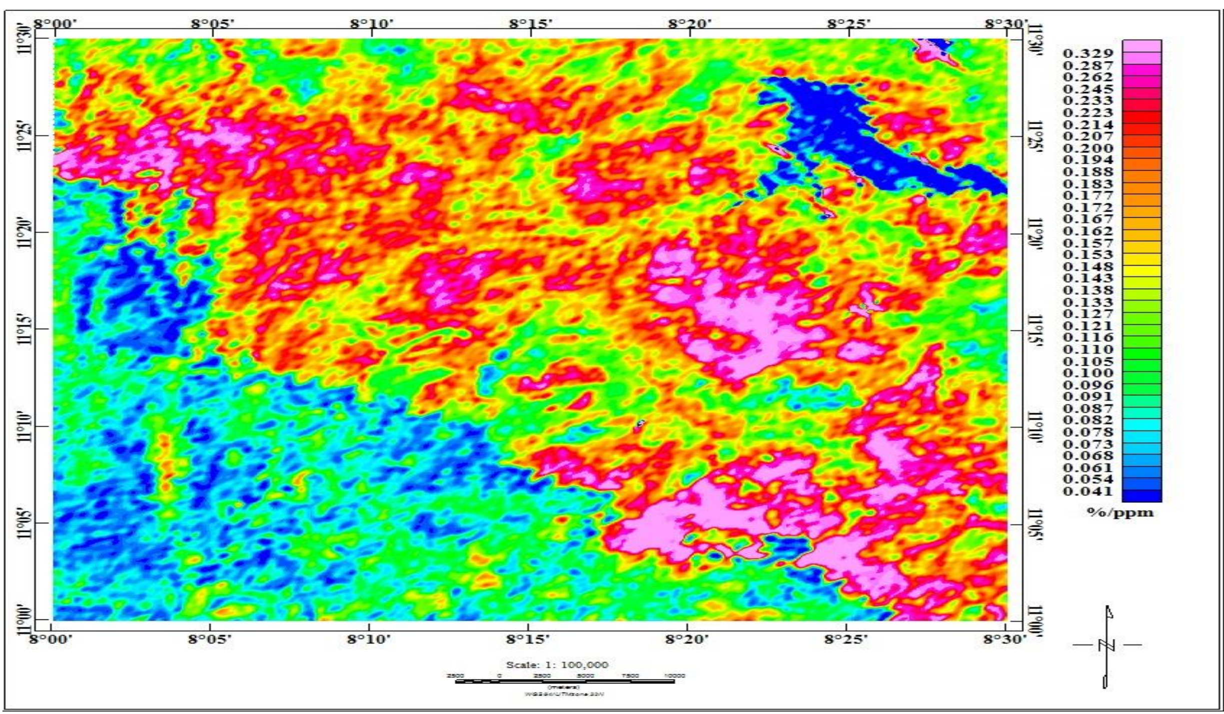

Fig. 9: Potassium/Thorium (%K/eTh) ratio map of study area

Regions with comparable Landsat and aerial gamma-ray data fingerprints were identified. After processing the Landsat and gamma ray data subsets independently, the findings indicate that the gamma ray data fingerprints are nearly entirely reflected in these derivative anomalies. These anomalies matched the sites of potential mineral deposits in the research region as well as several geologic features.

Thus they offer potential candidates for additional research.

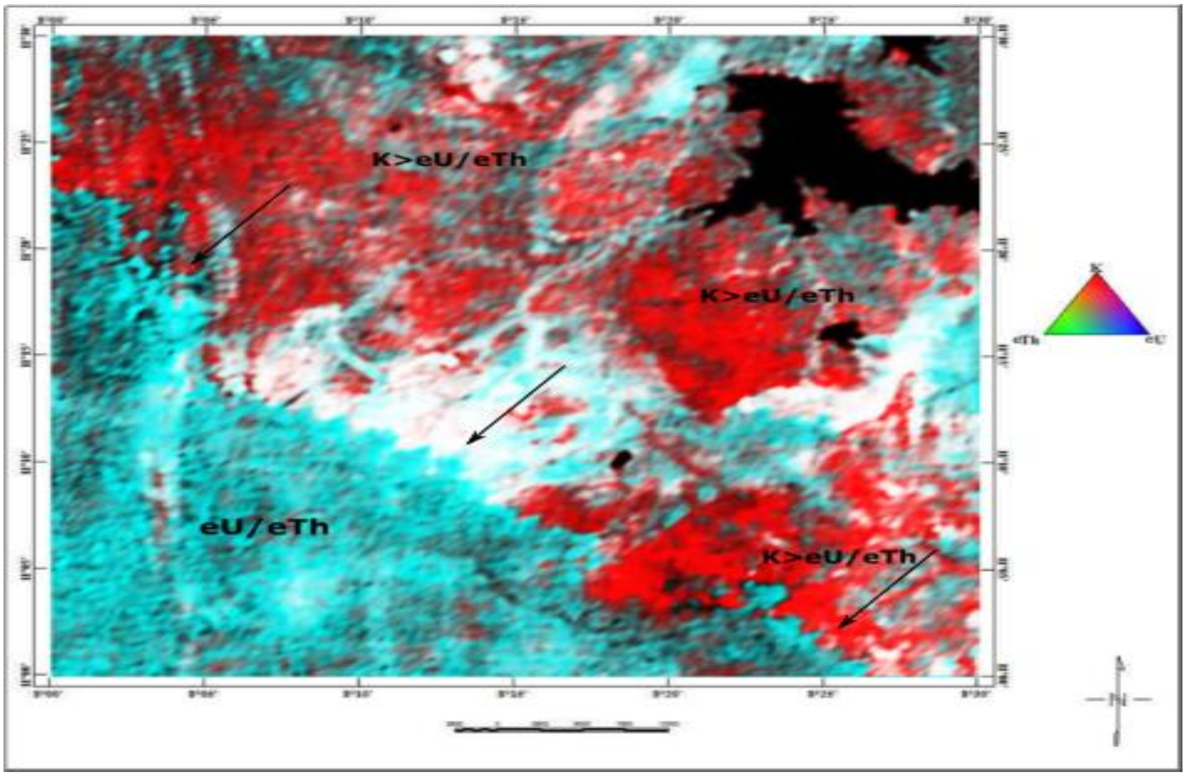

Fig. 10: Ternary image of RGB colour model and histogram equalizer as shading grid colour.

3.0 Conclusion

Lithologies and zones with high, moderate, and low concentrations of naturally occurring radioelements (uranium (eU), thorium (eTh), and potassium (K)) were distinguished using Landsat-8 OLI and aeroradiometric data, respectively. A potential NW-SE trending regional fracture created a clear segregation in the lithologies. Additionally, this led to the distinct separation of areas with elevated eU/eTh concentrations from those with elevated potassium concentrations. As a result, the distribution patterns of the K, eU, and eTh anomalies varied significantly. The potassium concentration was in (%) while that of uranium and thorium were in (ppm). K/eTh map showed regions of hydrothermal zone which were observed to be around the suspected NW-SE regional fracture. Areas further away from the regional fracture were identified as moderate to low hydrothermal zones. Ternary images were very useful in discriminating rock units within the study area. The reddish zones were identified to be underlain by medium to course biotite granite rocks; the blueish zones were underlain by migmatites and the blackish zones by porphyritic biotite-hornblende granite with gneissic rocks towards the east. These elements are not in minable quantities nor in form of ores. U/Th was higher in the rock units in the southern parts of the location studied. This was as a result of the dominance of the granitoids with U/Th affinity accessory minerals; and possibly as a result of their high affinity to water, leaching from natural deposits, and probably high usage of phosphate fertilizer containing uranium. The major and subsidiary fractures in the study area may have evolved during a regional tectonic movement or reactivation of a regional fault.

4.0 Reference

Agboola, G., Beni, L. H., Elbayoumi, T., & Thompson, G. (2024). Optimizing landslide susceptibility mapping using machine learning and geospatial techniques. *Ecological Informatics*, *81*, 102583. https://doi.org/10.1016/j.ecoinf.2024.102583

Ahmed, S. B. (2018) Integration of airborne geophysical and satellite imagery data to delineate the gasradioactive zones at west Safaga Area, Eastern Desert, Egypt. *NRIAG J Astron Geophysics*. *7(2)*, 297–308.

Ajibade, A. C. & Wright, J. B. (1989). The Togo-Benin-Nigeria shield: evidence of crustal aggregation in Pan-African belt. *Tectonophysics*: *165*, 125-129 and 433-449.

Amarachukwu Bernaldine Isiaka, Vivian Nonyelum Anakwenze, Chiamaka Rosemary Ilodinso, Chikodili Gladys Anaukwu, Chukwuebuka Mary-Vin Ezeokoli, Samuel Mensah Noi, Gazali Oluwasegun Agboola, & Richard Mensah Adonu. (2024). Harnessing Artificial Intelligence for Early Detection and Management of Infectious Disease Outbreaks. *International Journal of Innovative Research and Development*. https://doi.org/10.24940/ijird/2024/v13/i2/FEB24016

Aminu, M. B., Nanfa, C. A., Hassan, J. I., Yahuza, I., Christopher, S. D., & Aigbadon, G. O. (2022a). Application of Electrical Resistivity for Evaluation of Groundwater Occurrence within Adankolo Campus and Environs, Lokoja North Central, Nigeria. *European Journal of Environment and Earth Sciences*, *3*(1), 14–22. https://doi.org/10.24018/ejgeo.2022.3.1.235

Aminu, M. B., Christopher, S. D., Nanfa, C. A., Dahiru, A. T., Yohanna, A., Musa, N., & Tobias, S. (2022b). Petrography and Heavy Mineral Studies of Lokoja Formation along Mount Patti North Central Nigeria: Implication for provenance Studies. *European Journal of Environment and Earth Sciences*, *3*(2), 36–51. https://doi.org/10.24018/ejgeo.2022.3.2.243

Ball, E. (1980). An example of very consistent brittle deformation over a wide intracontinental area: The Late Pan-African fracture system of the Taureg and Nigerian shield. *Tectonophysics*: *16*, 363-379.

Black, R., Ball, E., Bertrand, J. M. L., Boullier, A.M., Caby, R., Davison, I., Fabre, J., Leblanc, M. and Wright, L.I. (1979). Outline of the Pan-African geology of Adrar des Iforas (rep. of Mall). *Geol. Rundsch*. *68*(2): 543-564.

Black, R., Latouche, L., Liegeois, J. P., Caby, R. & Bertrand, J.M. (1994). Pan African displaced terranes in the Taureg shield (Central Sahara). Geology (22): 641-644.

Boullier, A. M. (1991). *The Pan-African Tran-Saharan belt in the Hoggar shield (Algeria, Mali.Niger): a review. In:* DALLMEYER, R.D. &LEC'ORC'HE, J.P. (editors) The West African Orogens and Circum-AtlanticCorrelatives. Springer-Verlag, Berlin, pp.85-105.

Burke, K.C. and Dewey, J.F. (1972). Orogeny in Africa; In: African Geology, edited by Dessauvagie, T.F.J. and Whiteman, A.J. University of Ibadan. Pp. 583-608.

Caby, R., Bertrand, J.M.L. & Black, R. (1981). *Pan-African ocean closure and continental collision in the Hoggar-Iforas segment Central Sahara*: In Precambrian Plate Tectonics. Kröner, A. (Editor); Elsevier Amsterdam, pp. 407-434.

Caby, R. (1989). Precambrian terranes of Benin- Nigeria and northeast Brazil and the late Proterozoic South Atlantic fit. Geological Society America Special Paper (**230**), pp. 145-158.

Chijioke-Churuba, J. (2023). Energy Sustainability: Bridging the Gap between

Oil and Gas Operations and Community Well-Being in the Niger Delta Region, Nigeria. *Journal of Applied Sciences and Environmental Management*, *27*(11), 2503–2507

Chijioke-Churuba, J. (2024). Resilience Planning for Oil and Gas Communities in Response to Climate Change: Preparing Stakeholders for Future Challenges. *Journal of Management Science and Career Development*, *6*(7). https://ssaapublications.com/sjmscd/article/view/414

Dahuwa, D., Umar, W., Sani, M. and Abba, L. (2018). Aeromagnetic data analysis of tafawa balewa area using second vertical derivative and analytic signal techniques. IOSR *Journal of Applied Geology and Geophysics (IOSR-JAGG), 6(1),* 25-32.

Dickson, B. L. & Scott, K.M., 1997: Interpretation of Aerial Gamma-ray Surveys- Adding the Geochemical Factors. *AGSO Journal of Australian Geology and Geophysics, 17(2), pp. 187 – 200*

Dobrin, M. B. (1976), *Introduction to Geophysical Prospecting*. Mc-Graw Hill Books Co (3rd Ed.) N.Y. Pp. 630.

Elkhateeb, S. O. & Abdellatif, M. A. G. (2018). Delineation potential gold mineralization zones in a part of Central Eastern Desert, Egypt using Airborne Magnetic and Radiometric data. NRIAG J Astron Geophys 7(2):361–376.

Fitches, R. W., Ajibade, A. C., Egbuniwe, I.G., Hole, R. W. & Wright, J. B. (1985). Late Proterozoic Schist Belts and Plutonism in Northwestern Nigeria: *Journal of Geological Society London*, *142*, 319-337.

Grant, N. K. (1970). Geochronology of Precambrian basement rocks from Ibadan, southwestern Nigeria. *Earth Planetary Science Letters*. *10*, 29-38.

Grant, N.K., Hickman, M., Burkholder, F.R. & Powell, J. L. (1972). Kibaran metamorphic belt in the Pan-African domain of West Africa, nature (London), *134*, 343-349.

Holt, R.W., Egbuniwe, I. G, Fitches, W.R. & Wright, J.B. (1978). The relationship between low grade metasedimentary belts, calc-alkaline volcanism and the Pan-African orogeny in northwestern Nigeria: *GeologischeRundschau., 67*, 631-646.

Kettles, I. M., Rencz, A. N. & Bauke, S. D 2000. Integrating Landsat, Geologic, and Airborne Gamma Ray Data as an Aid to Surficial Geology Mapping and Mineral Exploration in the Manitouwadge Area, Ontario. *Photogrammetric Engineering & Remote Sensing 66(4),* 437-445.

Lawal, T. O. (2020). Integrated aeromagnetic and aeroradiometric data for delineating lithologies, structures, and hydrothermal alteration zones in part of southwestern Nigeria. *Arabian Journal of Geosciences*., *13*(775), 1-19.

Leblanc, M. (1981). *The Late Proterozoic Ophiolites of BouAzzer (Morocco) evidence for Pan-African plate tectonics*: In Precambrian Plate Tectonics. Kroner, A. (Editor): *Elsevier,* Amsterdam. P. 435-451.

Maged, M., Mansor, S. & Hashim, M. (2009). Geologic mapping of United Arab Emirates using multispectral remotely sensed data. *Amer. J. Eng. Appl. Sci*. *2*, 476-480.

McCurry, P. (1976). *The Geology of the Precambrian Palaeozoic rocks of Northern Nigeria- review*. In: C.A. Kogbe (Editor), Geology of Nigeria. Elizabethan Publishers and Co., Lagos, pp. 15-39.

McCurry, P. & Wright, J. B. (1977). Geochemistry of calc-alkaline volcanics in northwestern Nigeria and a possible Pan-African suture zone: *Earth Planetary Science Letter*, *37*, 90-96.

Nanfa, C. A., Aminu, M. B., Christopher, S. D., Akudo, E. O., Musa, K. O., Aigbadon, G. O., & Millicent, O. I. (2022.). Electric resistivity for Evaluating Groundwater

Potential along the Drainage zones in the Part of Jos North, Plateau State, Nigeria. *European Journal of Environment and Earth Sciences*. *3*(6), 59-68.

Ogungbemi, O. S., Amigun, J. O. & Olayanju, G. M. (2018). Geophysical characterization of mineralization potential of eastern parts of Ife-Ijesha Schist-Belt, southwestern Nigeria. *International Journal of Science and Technology Research*, 7(3), 21–27.

Ostrovskiy, E. A. (1975). Antagonism of radioactive elements in well rock alteration fields and its use in aerogamma spectrometric prospecting. *Int Geol Rev 17*, 461–468. https://doi.org/10.1080/00206817509471687.

Oversby, V. M. (1975). Lead isotope study of aplites from the Precambrian rocks near Ibadan, Southwestern Nigeria. *Earth Planetary Science Letters*, *7*, 177-180.

Salem, A., Abouelhoda, E., Alaa, A., Atef, I., Sachio, E. & Keisuke, U. (2005). *Mapping Radioactive Heat Production from Airborne Spectral Gamma-Ray Data of Gebel Duwi Area, Egypt.* Proceedings World Geothermal Congress, Antalya, Turkey, pp. 24-29.

Semere, S. & Ghebreab, W. (2006). Lineament characterization and their tectonic significance using Landsat TM data and field studies in the central highlands of Eritrea. J. Afr. Earth Sci., *46(4)*, 371-378.

Silva, A. M., Pires, A. C. B., Mccafferty, A., de Moraes, R. A. V. & Xia, H. (2003). Application of airborne geophysical data to mineral exploration in the uneven exposed terrains of the Rio Das Velhas Greenstone Belt. *Revista Brasileirade Geociências, 33(2)*, 17–28.

Turner, D. C. (1983). Upper Proterozoic schist belts in the Nigerian sector of the Pan-African province of West Africa: *Precambrian Research*, *21*, 55-79.

Wemegah, D. D., Preko, K., Noye, R. M., Boadi, B., Menyeh, A., Danuor, S. K. & Amenyoh, T. (2015) Geophysical interpretation of possible gold mineralization zones in Kyerano, South-Western Ghana using aeromagnetic and radiometric datasets. *J Geosci Environ Prot 3*, 67–82.

Woakes, M., Rahaman, M. A. & Ajibade, A. C. (1987). Some metallogenic features of the Nigerian Basement. *Journal of African Earth Sciences, 6(5)*, 655-664.

Wright, J. B., Hastings, D. A, Jones, W. B& Williams, H. R. (1985). Geology and mineral resources of West Africa. *George Allen &Unwin, London*, ***187***, pp. 111-123.

Youssef, M. A. S. & Elkhodary, S. T. (2013) Utilization of airborne gamma ray spectrometric data for geological mapping, radioactive mineral exploration and environmental monitoring of southeastern Aswan city, South Eastern Desert, Egypt. *Geophys J Int. Oxford University Press 195(3)*, 689–1700

Acknowledgement

I will like to thank the NGSA for making available the aeroradiometric datasets needed to carry out this study.

Compliance with Ethical Standards Declaration

Ethical Approval

Not Applicable

Competing interests

The authors declare that they have no known competing financial interests

Funding

All aspect of the work was carried out by the author

Authors' Contribution

NFA designed and coordinated the work and also joined MBA & CSN to write the first draft. All the authors were involved in the field work.